Optimized Design of Multilayer Barrier Films Incorporating a Reactive Layer. III. Case Analysis and Generalized Multilayer Solutions

Stanislav E. Solovyov, Anatoliy Y. Goldman

Department of Materials and Processing, Alcoa Closure Systems International, Incorporated, 1205 Elmore Street, Crawfordsville, Indiana 47933

Received 25 October 2004; accepted 30 August 2005
DOI 10.1002/app.23440
Published online 3 February 2006 in Wiley InterScience (www.interscience.wiley.com).

ABSTRACT: In part III of this series of articles, we present the analysis of transient permeation through two-layer reactive–passive (RP) film designs, the analysis extension to multilayer structures, and optimized design solutions for multilayer barriers incorporating immobile noncatalytic oxygen scavenger within one of the layers. The reduction of oxygen ingress into a package within a certain timeframe depends on two factors: extension of the scavenger exhaustion time and reduction of the transient transmission rate through the film during that time. The optimal design for the scavenger exhaustion time involves exposure of the reactive layer to the package contents and its protection from high levels of environmental oxygen by the best possible passive barrier layer. The film barrier properties can be further optimized by the selection of the matrix material to place the scavenger in. Reducing the initial transmission rate requires the placement of the scavenger within a layer with the lowest diffusivity of the matrix polymer. When one chooses between two layers with different material transport properties in which to put the scavenger, the optimal solution for the ingress depends on the desired time to provide an improved barrier. The lifetime of the scavenger in the RP film is shortened for design 1, when the diffusivity of the reactive layer is smaller than that of the passive layer, compared to RP design 2, with the layer matrix sequence reversed, but the transient transmission rate is greatly reduced on average for the former. If the desired time to provide a barrier does not exceed the scavenger exhaustion time for RP design 1, the lowest diffusivity material should be used as a matrix for the innermost layer loaded with the scavenger. Otherwise, the highest possible passive barrier should be placed into the film external layer to minimize the total ingress during longer times. J Appl Polym Sci 100: 1966–1977, 2006

Key words: permeable; reactive; barrier; membranes

INTRODUCTION

In parts I and II[1,2] of this series, we introduced the extension of the Solovyov–Goldman (SG) model of transient permeation through the noncatalytic reactive membrane[3–5] to two-layer reactive–passive (RP) structures [hereafter, known as the extended Solovyov–Goldman (ESG) model]. The model was applied to the analysis of environmental oxygen ingress dynamics into a sealed package with zero initial partial oxygen pressure inside ($p_{in} = 0$), positive partial pressure outside ($p_{out} > p_{in}$), and the noncatalytic (consumable) oxygen scavenger dispersed in one layer of the packaging film. The choice of the boundary conditions allowed us to focus on the unidirectional ingress into the package only and to avoid considering the complicated effects of potential oxygen reduction in the package headspace due to the scavenging reaction in the film.

Figure 1 demonstrates typical partial pressure profiles of the permeating solute in the RP and passive–reactive (PR) films at the moment of uniform scavenger activation throughout the reactive layer at $t = 0$ (dashed lines) and at $t = \infty$ (solid lines) when the capacity of the film to scavenge dissolved oxygen is completely depleted by the reaction [the passive–passive (PP) film]. The solute ingress dynamics with corresponding lag times is shown in Figure 2 for the single-layer noncatalytic reactive and passive films at reference and steady-state initial conditions. The solid lines represent actual ingress at the steady-state initial conditions, and the SG model is a combination of transient ingress through the reactive film before the scavenger exhaustion time (t_E°) estimate and the ingress through the passive film after that time (dotted lines). t_{LR}^{SS} is the steady-state reactive lag time for initial Thiele modulus (ϕ_0) values greater than zero, and t_L^+ is the corresponding SG model steady-state lag time for intermediate values of $\phi_0 > 2$ and serves as an engineering barrier performance estimate, at times comparable to t_E°.

Correspondence to: S. E. Solovyov, Multisorb Technologies, Incorporated, 325 Harlem Road, Buffalo, NY 14224 (ssolovyov@multisorb.com).

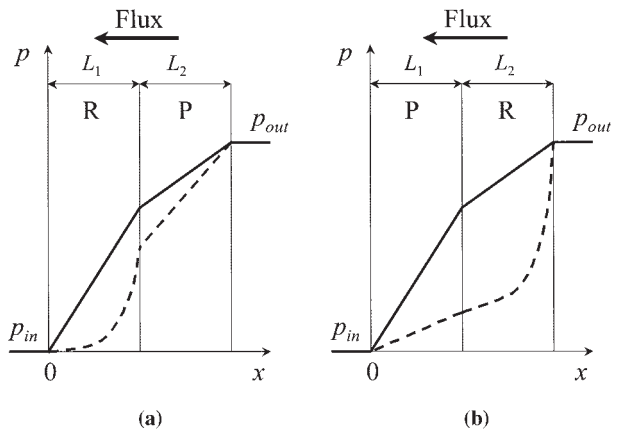

Figure 1 Typical solute partial pressure profiles in the (a) RP and (b) PR films at (- - -) the moment of the scavenger activation and (—) after complete exhaustion of the scavenger reactive capacity (for steady-state permeation across the PP film).

In the following text, the terminology and notation continue from parts I and II of this series.

CASE ANALYSIS

We reproduce the scaling parameters [eq. (12) from part I] corresponding to $\phi_0 = 1$ in the reactive layer and the solute partial pressure difference of 0.2 atm, representing oxygen in ambient air outside and no free oxygen inside the package (maintained):

Layer thickness: $L = 10^{-4}$ m

Oxygen diffusivity in the layer: $D = 10^{-12}\text{m}^2/\text{s}$

Oxygen solubility in the layer:

$$S = 10^{-6}\text{m}^3(\text{STP})\text{m}^{-3}\text{Pa}^{-1}$$

Apparent initial reaction rate: $k_0 = \mu K R_0 = 10^{-4}\text{s}^{-1}$

Scavenging capacity of the film material:

$$\mu R_0 = 1\ \text{m}^3(\text{STP})/\text{m}^3$$

Oxygen flux (note negative flux scaling):

$$J = -10^{-10}\text{m}^3(\text{STP})\text{m}^{-2}\text{s}^{-1}$$

These values do not represent any particular polymer film properties or scavenger chemistry. They were selected for convenience purposes only, although they do reflect some typical polymer properties found in commercial packaging films. The scavenging capacity of the film material loaded with the scavenger was chosen to be relatively low compared to currently available systems. As a result, the actual barrier improvement with higher capacity scavengers may last for months rather than days, as reported in the tables and figures for methodology demonstration purposes only.

All variables reported in the tables and figures include dimensionless parameter values normalized to values in eq. (12) of part I. First, we analyze two-layer laminates from different polymeric materials where one layer contains an oxygen scavenger and observe the effects of material properties and scavenger placement on the initial barrier improvement (when the scavenger capacity is at its maximum immediately on activation throughout the reactive layer). Then, we apply eqs. (16) and (25) from part I of the series to calculate the total oxygen ingress through the structure during any time $t \le t^{\circ}_E$. All ingress after that time can be assumed to occur through a purely passive barrier, and it is easily found from eq. (24) of part I.

In the following tables, $J_0(0)$ is the initial effective flux through the RP film (determined at the downstream boundary $x = 0$), J^{PP} is the steady-state flux through the reference two-layer PP film without the scavenger, $\gamma\,[= J^{PP}/J_0(0)]$ is the initial barrier improvement ratio for the film with the reactive layer upon scavenger activation, and μR_0 is the material scavenging capacity and is equal to 1 m^3 (STP)/m^3, except where noted otherwise. Exhaustion and lag times are reported in days rather than the usually reported dimensionless units normalized to the reference lag time for passive barriers (t_L) to provide a proper engineering perspective. The reasoning for this choice follows from eq. (34) of part I, which shows the proper scaling as a product of the relative scavenging capacity (Ψ) of the film and t_L rather than t_L alone.

Table I is an expanded version of our earlier results[4] for the homogeneous noncatalytic homogeneous reactive layer. In the table, $J_0(0)$ denotes the initial effective flux through the reactive film, J^P is the steady-state

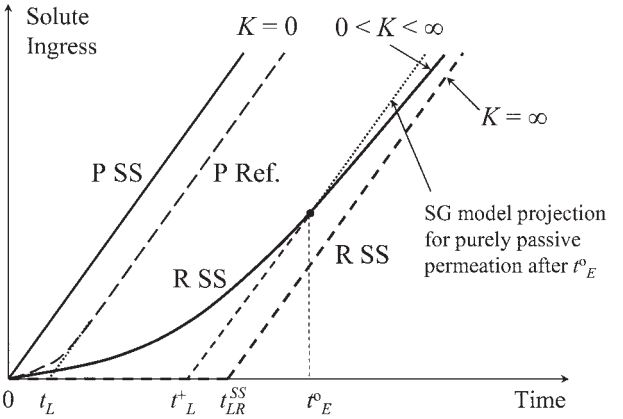

Figure 2 Relationship between reference (Ref.), steady-state (SS), and SG model lag times in the noncatalytic reactive monolayer (R = reactive layer; P = passive layer).

TABLE I
Reactive Film with $\mu R_0 = 1$ m³(STP)/m³, Except for Case 7, for Which $\mu R_0 = 0.5$

	Reactive layer properties					Performance properties									
Case	D	S	L	k_0	ϕ_0	Ψ	J_0 (0)	J^P	γ	t_{LR}^{SS}	t_E°	I_R (t_E°)	I_P (t_E°)	ε	t_L^+
1	1	1	1	10	3.162	50	5.36×10^{-1}	2	3.729	2.894	4.323	42.66	74.71	1.751	1.855
2	0.1	10	1	10	10	5	1.82×10^{-3}	2	1101.3	2.894	3.432	15.19	59.31	3.905	2.553
3	10	0.1	1	10	1[b]	500	1.702	2	1.175	2.894	5.404	60.89[c]	93.38	1.534[d]	1.880
4	0.1	1	1	10	10	50	1.82×10^{-4}	0.2	1101.3	28.94	34.32	15.19	59.31	3.905	25.53
5	1	0.1	1	10	3.162	500	5.36×10^{-2}	0.2	3.729	28.94	43.23	42.66	74.71	1.751	18.55
6	0.1	0.1	1	10	10	500	1.82×10^{-5}	0.02	1101.3	289.4	343.2	15.19	59.31	3.905	255.3
7[a]	1	1	2	5	4.472	25	1.02×10^{-1}	1	9.786	5.787	7.974	32.28	68.90	2.134	4.238
8	1	1	2	10	6.325	50	2.27×10^{-2}	1	44.12	11.57	14.83	47.10	128.16	2.721	9.382
9	1	1	1	100	10	50	1.82×10^{-3}	2	1101.3	2.894	3.432	15.19	59.31	3.905	2.553
10	1	1	1	1000	31.62	50	2.34×10^{-13}	2	8.6×10^{11}	2.894	3.073	4.91	53.09	10.81	2.788

The total solute scavenging capacity of the film was the same constant $\mu R_0 AL$ for all cases except 8, for which it was doubled.

[a] μ was the same, and R_0 was reduced by 50% to keep the total load constant. $\mu R_0 = 0.5$.

[b] $\phi_0 < 2$ is out of the validity range of the SG model.

[c] Ingress underpredicted by the SG model.

[d] ε overpredicted because of the error in the ingress estimate.

flux through the corresponding passive film (with $k = 0$), γ [$= J^P/J_0(0)$] is the initial barrier improvement ratio for the reactive film versus passive film, t_{LR}^{SS} is the steady-state reaction lag time (the Yang–Nuxoll–Cussler (YNC) lag time), t_E° is the SG model exhaustion time, $I_R(t_E^\circ)$ is the solute ingress through the reactive film during t_E° [cm³ (STP)/m²], $I_P(t_E^\circ)$ is the corresponding solute ingress through the passive film, ε is the cumulative barrier improvement ratio $I_R(t_E^\circ)/I_P(t_E^\circ)$ during t_E° due to the scavenging reaction, and t_L^+ is the SG model steady-state lag time estimate defined with the intersect of the passive ingress $I_P(t)$ slope at $t = t_E^\circ$ with the zero ingress axis, as in ref. 4, analogous to the asymptotic definition of t_L. Because t_E° is an estimate of the scavenger exhaustion time, t_L^+ taken at t_E° does not represent true asymptotic behavior. Following our earlier analysis,[4] the true asymptote is always given by t_{LR}^{SS} in eq. (31) of part I if ϕ_0 is not very close to zero and the film is not very thin. The point of introducing t_L^+ for real-world packaging applications is to estimate the barrier properties of RP structures on a timescale comparable to the scavenger exhaustion times rather than to be content with the asymptotic ingress analysis at an infinite time.

Comparing cases 1, 2, and 3, we observe that permeability ($P = DS$) of the passive films and the corresponding flux (J^P) values are the same, whereas the D and S values are varied. There is a large difference in $J_0(0)$ through reactive film, as demonstrated by γ. Material 2, with the lowest D, provides the best initial and transient barrier improvement (upon scavenger activation), whereas material 3, with the highest D, provides almost no improvement in terms of t_L^+ and significantly higher solute ingress I during a comparable t_E°. t_L^+ is also improved for material 2 compared to materials 1 and 3.

Cases 4–6 demonstrate the effects of separate changes in material parameters D and S. We can see that lowering D is again the preferred way of improving the transient performance of the noncatalytic reactive barrier. Apparently, lower diffusion rates translate into longer average passage times of the individual solute molecules across the reactive layer, which results in a higher likelihood of reaction with the scavenging sites. This effect far outweighs the negative effects of the increased oxygen solubility in the matrix.

Comparing cases 2 and 9, we note that increasing k_0 10-fold is equivalent to simultaneously reducing D and increasing S 10-fold, whereas comparing case 9 with case 1, we see a large increase in the transient barrier performance in case of a higher reaction rate accompanied by some extension of t_L^+ despite some shortening of t_E°.

Increasing the film thickness twofold, as shown in cases 7 and 8, with the same total amount of loaded scavenger per film (7 vs 1) and the same scavenger concentration in film (8 vs 1), respectively, leads to different results. In case 8, doubling the reactive film thickness reduces the initial solute flux by a factor $\sinh(2\phi_0)/\sinh(\phi_0)$ according to our findings in ref. 4 and dramatically increases the scavenger exhaustion time and the barrier improvement ratio. Here, ϕ_0 is the initial Thiele modulus of the reference film with $L = 1$. In case 7, dispersing the same amount of the scavenger as in case 1 in a film twice as thick lowers ϕ_0 and results in a less dramatic but still substantial barrier improvement.

TABLE II
RP Film with the Reactive Layer Exposed to the package Contents and the Passive Layer Exposed to the Environment

	Reactive layer			Passive layer				Performance properties								
Case	D_1	S_1	L_1	D_2	S_2	L_2	ϕ_0	J_0 (0)	J^{PP}	γ	t_{LR}^{SS}	t_E°	I_R (t_E°)	I_P (t_E°)	ε	t_L^+
1	1	1	1	1	1	1	3.16	1.29×10^{-1}	1.000	7.78	7.82	11.69	42.66	101.01	2.368	6.75
2	1	1	1	0.1	1	1	3.16	1.64×10^{-2}	0.182	11.10	47.65	71.19	42.66	111.84	2.622	44.04
3	0.1	1	1	1	1	1	10.0	9.08×10^{-5}	0.182	2002.4	41.07	48.71	15.19	76.52	5.038	39.05
4	0.1	1	1	0.1	1	1	10.0	1.65×10^{-5}	0.100	6057.3	97.93	116.16	15.19	100.37	6.608	98.58
5	1	0.1	1	1	1	1	3.16	4.07×10^{-2}	0.182	4.47	34.69	51.83	42.66	81.43	1.909	24.68
6	1	1	1	1	0.1	1	3.16	1.64×10^{-2}	0.182	11.10	47.65	71.19	42.66	111.84	2.622	44.04
7	1	0.1	1	1	0.1	1	3.16	1.29×10^{-2}	0.100	7.78	78.25	116.91	42.66	101.01	2.368	67.54
8	10	0.1	1	1	1	1	1.0[d]	7.36×10^{-1}	1.000	1.36	6.21	11.59	60.89[e]	100.16	1.645[f]	4.55
9	0.1	10	1	1	1	1	10.0	1.65×10^{-4}	1.000	6057.3	9.79	11.62	15.19	100.37	6.608	9.86
10	0.1	10	1	0.1	10	1	10.0	1.65×10^{-4}	1.000	6057.3	9.79	11.62	15.19	100.37	6.608	9.86
11	0.1	10	1	0.1	1	1	10.0	1.80×10^{-5}	0.182	10112.2	57.41	68.09	15.19	106.96	7.043	58.42
12	10	0.1	1	0.1	1	1	1.0[d]	1.20×10^{-1}	0.182	1.51	35.79	66.85	60.89[e]	105.01	1.725[f]	28.09
13	1	1	1	1	1	2	3.16	7.30×10^{-2}	0.667	9.13	12.33	18.42	42.66	106.10	2.487	11.01
14[a]	1	1	2	1	1	1	4.47	3.16×10^{-2}	0.667	21.12	11.86	16.35	32.28	94.16	2.917	10.74
15[a]	1	1	2	1	1	2	4.47	1.87×10^{-2}	0.500	26.78	16.95	23.36	32.28	100.92	3.126	15.89
16[b]	1	1	1	1	1	1	3.16	1.29×10^{-1}	1.000	7.78	78.25	116.91	426.62	1010.13	2.368	67.54
17[c]	1	1	1	1	1	1	10.0	1.65×10^{-4}	1.000	6057.3	9.79	11.62	15.19	100.37	6.608	9.86

$k_1 = 10$, $k_2 = 0$, and $\mu R_0 = 1$, except as noted. The total scavenging capacity of the film was the same constant $\mu R_0 AL_1$ for all cases except 16.

[a] μ was the same; R_0 was reduced by 50% to keep the total load constant. $\mu R_0 = 0.5$.

[b] μ was increased 10-fold, and the scavenger load was constant. $\mu R_0 = 10$.

[c] The scavenger reactivity was increased 10-fold, and the scavenger load was constant. $k_1 = 100$.

[d] $\phi_0 < 2$ was out of the validity range of the SG model.

[e] Ingress underpredicted by the SG model.

[f] ε overpredicted because of the error in the ingress estimate

Reducing S in the film material 10-fold (cf. cases 1 and 5) does not affect γ but rather increases the scavenger lifetime proportionally to the solubility reduction factor to produce the same solute ingress.

Table II presents the performance of the RP film, that is, a two-layer structure with its reactive layer exposed to the package contents with $p_{in} = 0$ and a fixed interfacial solute concentration (C_1^*), found according to eq. (38) of part II. Table III shows the PR film results for comparison. Note that approximate calculations of t_E° for the wavefront propagation in Table III were performed with the assumption that the interfacial solute concentration $C_2 = 0$ in the reactive layer for the reaction wavefront dynamics and with the dynamic ingress scalability approach represented by the eq. (67) of part II.

Comparing the data in Tables II and III, we conclude that RP film design is superior to PR film in extending the scavenger lifetime, whereas γ does not depend on the layer sequence. Another important result is that placing the scavenger into a layer with the lowest diffusivity produces the best initial barrier compared to placing it into high diffusivity material and protecting it from environmental oxygen by a high passive barrier layer (cf. cases 2 and 3 in Table II).

When case pairs 2–6 and 9–10 in both Tables II and III are compared, it is easy to conclude that the nature of the passive layer does not affect any performance properties of the RP and PR films, provided the steady-state transmission rate ($TR = DS/L$) of the passive layer is the same. Thus, we can extend the results of our analysis to structures containing arbitrary single-layer and multilayer passive barrier sequences before and after the active layer and characterize them only by their respective overall transmission rate (permeance) of the particular solute at chosen conditions.

Figure 3 exemplifies the oxygen ingress through the reactive and passive homogeneous films found according to eq. (28) of part I for the reactive film with noncatalytic scavenger turning into the passive film during t_E° as a function of the initial Thiele modulus and eq. (24) of part I for passive film. At each value of ϕ_0, the ingress during a fixed t_E° is compared for the passive and reactive films. For the reactive film, the t_E° represents the approximate scavenger exhaustion time, whereas for the passive film, the same time is used as a baseline for comparison purposes. t_E° itself depends on ϕ_0 of the reactive film as noted; hence, the ingress through passive film is seen as a nonlinear function of ϕ_0 even though the passive film obviously exhibits linear dependence of the ingress on time when the steady-state initial conditions [eq. (7) of part I] are used. We note that the SG model solution for the reactive film provides excellent agreement with numerical simulation results only for $\phi_0 > 2$ because of

TABLE III
PR Film with the Passive Layer Exposed to the Package Contents and the Reactive Layer Exposed to the Environment

	Passive layer			Reactive layer				Performance properties								
Case	D_1	S_1	L_1	D_2	S_2	L_2	ϕ_0	J_0 (0)	J^{PP}	γ	t_{LR}^{SS}	t_E°	I_R (t_E°)	I_P (t_E°)	ε	t_L^+
1	1	1	1	1	1	1	3.16	1.29×10^{-1}	1.0000	7.78	2.89	4.62	19.00	39.9198	2.102	2.42
2	0.1	1	1	1	1	1	3.16	1.64×10^{-2}	0.1818	11.10	2.89	4.71	3.34	7.40	2.217	2.59
3	1	1	1	0.1	1	1	10.0	9.08×10^{-5}	0.1818	2002.4	28.94	34.32	13.80	53.92	3.907	25.54
4	0.1	1	1	0.1	1	1	10.0	1.65×10^{-5}	0.1000	6057.3	28.94	34.32	7.59	29.66	3.908	25.54
5	1	1	1	1	0.1	1	3.16	4.07×10^{-2}	0.1818	4.47	28.94	44.13	37.46	69.33	1.851	20.29
6	1	0.1	1	1	1	1	3.16	1.64×10^{-2}	0.1818	11.10	2.89	4.71	3.34	7.40	2.217	2.59
7	1	0.1	1	1	0.1	1	3.16	1.29×10^{-2}	0.1000	7.78	28.94	46.20	19.00	39.92	2.102	24.22
8	1	1	1	10	0.1	1	1.0[d]	7.36×10^{-1}	1.0000	1.36	2.89	8.55	32.06[e]	73.86	2.304[f]	4.84
9	1	1	1	0.1	10	1	10.0	1.65×10^{-4}	1.0000	6057.3	2.89	3.43	7.59	29.66	3.908	2.55
10	0.1	10	1	0.1	10	1	10.0	1.65×10^{-4}	1.0000	6057.3	2.89	3.43	7.59	29.66	3.908	2.55
11	0.1	1	1	0.1	10	1	10.0	1.80×10^{-5}	0.1818	10112.2	2.89	3.43	1.38	5.39	3.908	2.55
12	0.1	1	1	10	0.1	1	1.0[d]	1.20×10^{-1}	0.1818	1.51	2.89	13.58	5.58[e]	21.34	3.822[f]	10.03
13	1	1	2	1	1	1	3.16	7.30×10^{-2}	0.6667	9.13	2.89	4.66	12.45	26.86	2.158	2.50
14[a]	1	1	1	1	1	2	4.47	3.16×10^{-2}	0.6667	21.12	5.79	8.10	20.45	46.67	2.282	4.55
15[a]	1	1	2	1	1	2	4.47	1.87×10^{-2}	0.5000	26.78	5.79	8.13	15.19	35.10	2.311	4.61
16[b]	1	1	1	1	1	1	3.16	1.29×10^{-1}	1.0000	7.78	28.94	46.20	189.96	399.20	2.102	24.22
17[c]	1	1	1	1	1	1	10.0	1.65×10^{-4}	1.0000	6057.3	2.89	3.43	7.59	29.66	3.908	2.55

$k_1 = 0$, $k_2 = 10$ and $\mu R_0 = 1$, except as noted. The total scavenging capacity of the film was the same constant $\mu R_0 AL_2$ for all cases except 16.

[a] μ was the same, and R_0 was reduced by 50% to keep the total load constant. $\mu R_0 = 0.5$.

[b] μ was increased 10-fold, and the scavenger load was constant. $\mu R_0 = 10$.

[c] The scavenger reactivity was increased 10-fold, and the scavenger load was constant. $k_2 = 100$.

[d] $\phi_0 < 2$ was out of the validity range of the SG model for ingress.

[e] The ingress underpredicted by the SG model.

[f] ε overpredicted because of the error in the ingress estimate.

the reasons discussed in ref. 1. The numerical solution for the ingress (R-Num line, Fig. 3) also demonstrates the convergence of the reactive film and passive film solutions as $\phi_0 \to 0$. Figure 3 clarifies what kind of transient barrier performance during t_E° we can expect from the reactive film depending on the initial scavenger concentration (R_0) and the rate constant of its reaction with oxygen (K) through the initial Thiele modulus:

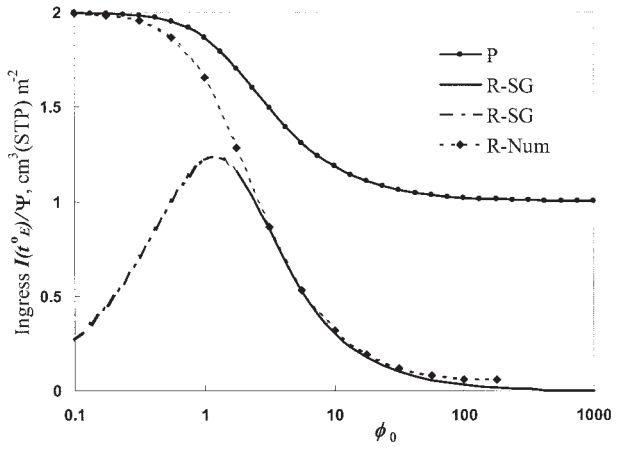

Figure 3 Oxygen ingress during t_E°.

$$\phi_0 = L\sqrt{\frac{\mu K R_0}{D}}$$

After that the passive barrier performance is determined from eq. (24) of part I. Note that the initial Thiele modulus in eq. (10) of part I refers to the initial L of the reactive layer: as the reaction wavefront propagates downstream, the reactive layer thickness [$L_d(t)$] is reduced, whereas R_0 in the reactive sublayer remains constant according to the SG model.

Figure 4 demonstrates the time dependence of the total oxygen ingress through the RP film found from eqs. (16) and (28) of part I for cases 1–4 in Table II and an additional case 5 with high diffusivity of the passive layer. These results were obtained with the fixed interfacial solute concentration approximation [eq. (38) of part II]. The longest t_L for the reference PP film is much shorter than 1 day, and its effect is negligible compared to t_E°, as shown in Table III for $p_{in} = 0$ and $p_{out} = 0.2$ atm [cf. corresponding Ψ values for the reactive layer calculated with C_1^* instead of the equilibrium concentration of the solute outside the package (C_{out}) with 1 to verify that statement]. The RP film parameters for Figure 4 are listed in Table IV.

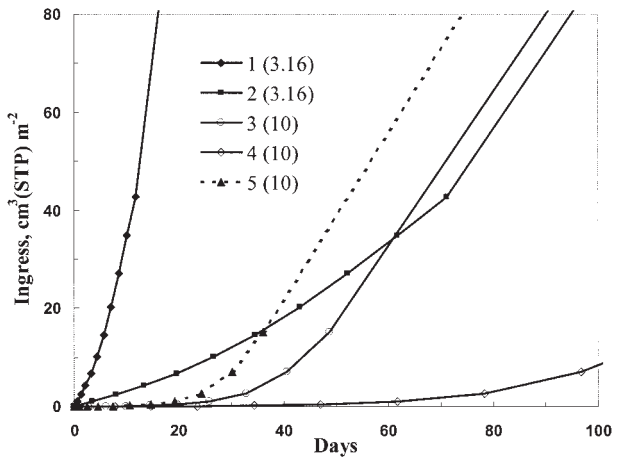

(a)

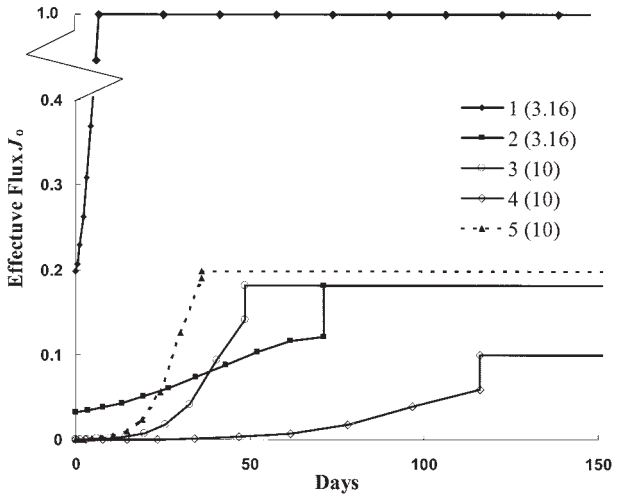

(b)

Figure 4 The (a) ingress and (b) J_0 dependence on time for the RP films. For all films, $k_1 = 10$, $k_2 = 0$, $\mu R_0 = 1$ m^3 (STP)/m^3, $L_1 = L_2 = 1$, and $S_1 = S_2 = 1$. The notation used in the legend is the case number from Table IV (ϕ_1), where ϕ_1 is the initial Thiele modulus for the reactive layer 1.

In Table IV $L_1 = L_2 = 1$ and $S_1 = S_2 = 1$. t_L for the PP film was calculated according to a formula reported by Siegel[6] that was originally derived by Barrie et al.:[7]

$$t_L^{(12)} = \frac{\dfrac{L_1}{S_1D_1}\left(\dfrac{L_1^2}{6D_1} + \dfrac{L_2^2}{2D_2}\right) + \dfrac{L_2}{S_2D_2}\left(\dfrac{L_2^2}{6D_2} + \dfrac{L_1^2}{2D_1}\right)}{\dfrac{L_1}{S_1D_1} + \dfrac{L_2}{S_2D_2}} \quad (1)$$

Recall that t_E° is defined as the approximate time of complete exhaustion of the scavenger reactive capacity rather than the time axis intercept of asymptotic solute concentration growth downstream (as is the case for t_L) at steady-state initial conditions for the solute dissolved in the film (vs initially solute free film for t_L). In the YNC model,[8] t_{LR}^{SS} (which is a limiting case of the steady-state t_E° at $\phi_0 \to \infty$) was erroneously compared with t_L rather than t_L^{SS} without distinction between the reference and steady-state lag times. The YNC model also assumed zero oxygen ingress (an impermeable reaction wavefront) until the scavenger capacity was completely exhausted by the propagating wavefront. In the SG model, the reaction wavefront is semipermeable; hence, we see the nonzero permeant ingress before the scavenger capacity is exhausted. The following section clarifies the differences in lag time definitions.

GENERALIZED REFERENCE AND STEADY-STATE LAG TIMES

We can define the reference lag time for the reactive film through its exhaustion lag time the same way as it is done for passive barriers (i.e., as the time axis intercept of downstream concentration $\{[C]_{in}(t)\}$ growth asymptotic outside the initially solute free film). It is convenient, however, to consider the steady-state lag time first, that is, the lag time defined for the reactive film where steady-state permeation across initially passive (inactivated) layer is already

TABLE IV
RP Film Parameters for Figure 4

			PP				SG	RP	
No.	Reactive D_1	Passive D_2	J^{PP}	t_L (days)	C_1/C_{out}	RP $C_1(0)/C_{out}$	average C_1^*/C_{out}	t°_E (days)	t_L^+ (days)
1	1	1	1.0000	0.0772	0.5000	0.2396	0.3698	11.69	6.75
2	1	0.1	0.1818	0.2823	0.0909	0.0305	0.0607	71.19	44.04
3	0.1	1	0.1818	0.2823	0.9091	0.5000	0.7045	48.71	39.05
4	0.1	0.1	0.1000	0.7716	0.5000	0.0909	0.2955	116.16	98.58
5	0.1	10	0.1980	0.2025	0.9901	0.9091	0.9496	36.14	27.27

C_1 = steady-state solute concentration on the layer 1 boundary of the PP interface; $C_1(0)$ = initial solute concentration in the reactive layer boundary of the RP interface obtained from the SG model for the catalytic scavenger; C_1^* = SG model solute concentration on the R side of the RP interface, which was assumed to be constant throughout the reaction.

established by $t = 0$. At $t = 0$, the scavenger is instantly activated throughout the layer, and the layer starts to consume the diffusing solute in addition to the solute initially present in the film.

The slope of the linear part of $[C]_{in}(t)$ inside the package adjusted by the downstream chamber volume over the barrier area is the value of the flux (J_x) across passive film found according to eq. (23) of part I, where TR is the steady-state transmission rate through the homogeneous single-layer membrane:

$$TR = \frac{P}{L} = \frac{DS}{L} \tag{2}$$

For the laminate with N passive layers, the steady-state transmission rate is found as in refs. 9 and 10:

$$TR_{1\ldots N} = \frac{1}{\dfrac{1}{TR_1} + \dfrac{1}{TR_2} + \cdots + \dfrac{1}{TR_N}} \tag{3}$$

The t_L^+ estimate for the noncatalytic reactive film has to asymptotically satisfy the equation of $[C]_{in}$ growth for $t > t_L^+$, that is, for $t \to \infty$:

$$[C]_{in}(t)\frac{V}{A} = I(t) = |J_x|(t - t_L^+) \tag{4}$$

provided $[C]_{in} \ll [C]_{out}$ and V is large so that $[C]_{in}(t)$ growth with time does not significantly affect the concentration difference $\Delta C = [C]_{out} - [C]_{in}$ that is a driving force for permeation and is assumed to be constant. Here, V is the volume of the downstream chamber, $[C]_{in}$ is the solute concentration in the chamber, A is the area of the barrier, and J_x is the steady-state solute flux across the passive (completely exhausted) barrier, which is the same at any position $x = [0 \ldots L]$. We use the absolute value of J_x to avoid carrying the negative sign in the equations, which is always the case when the $p_{in} < p_{out}$ condition is imposed. Figure 5 demonstrates the relationship between steady-state lag times and exhaustion lag times for the monolayer homogeneous film with the same thickness and matrix material properties D and S but different k_0 values for the initial scavenger loading. Case $k_0 = 0$ corresponds to the passive film with $t_L^{SS} = 0$, whereas case $k_0 = \infty$ corresponds to the YNC model for the reactive film with a finite reactive capacity and an instantaneous reaction.

Substituting $t = t_E^\circ$ into eq. (4) we obtain an engineering estimate for t_L^+, assuming that t_E° rather than $t = \infty$ represents the time frame of interest for taking the lag time asymptote:

$$t_L^+ = t_E{}^\circ - \frac{I(t_E{}^\circ)}{|J_x|} \tag{5}$$

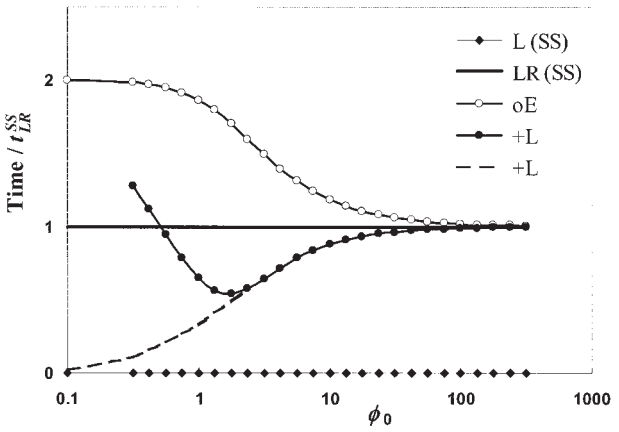

Figure 5 Relationship between steady-state lag times for the passive and reactive monolayer membranes and exhaustion lag times for reactive film: L (SS) = $t_L^{SS} \equiv 0$ for the passive membrane; LR (SS) = YNC lag time t_{LR} for the noncatalytic reactive monolayer; oE = t_E°; +L = t_L^+ for the noncatalytic reactive monolayer. (- - -) Projected t_L^+ behavior as $\phi_0 \to 0$.

For the monolayer reactive film, we substitute eqs. (17), (22), and eq. (29) of part I into eq. (5) to obtain results for the case of $p_{in} = 0$:

$$t_L^+ = \frac{\mu R_0}{k_0 S p_{out}}\left[\frac{\phi_0^2}{2} + \ln(\cosh(\phi_0)) - \frac{2\phi_0^2}{(1+\phi_0)}\left(\arctan(e^{\phi_0}) - \frac{\pi}{4} - \frac{e^{\phi_0}}{\phi_0(1+e^{2\phi_0})} + \frac{1}{2\phi_0}\right)\right] \tag{6}$$

For the two-layer RP film, the approximate expression is

$$t_L^+ = \frac{\mu R_0}{k_1 C_1}\left[\frac{\phi_1^2}{2} + \ln(\cosh(\phi_1))\right] - \frac{2\mu R_0 L_1}{(1+\phi_1)p_{out}}\left(\arctan(e^{\phi_1}) - \frac{\pi}{4} - \frac{e^{\phi_1}}{\phi_1(1+e^{2\phi_1})} + \frac{1}{2\phi_1}\right) \times \left(\frac{L_1}{S_1 D_1} + \frac{L_2}{S_2 D_2}\right) \tag{7}$$

Although C_1 does evolve in time, a good engineering approximation for it is the fixed C_1^* value that can be found from eq. (38) of part II with eqs. (2) and (9) of part II.

Assuming $C_2 = 0$, with eq. (67) of part II to find $I_{PR}^+(t_E^\circ)$ and substituting it into eq. (5) we obtain for the PR film

$$t_L^+ = \frac{\mu R_0}{k_2 C_{out}}\left[\frac{\phi_2^2}{2} + \ln(\cosh(\phi_2))\right] - \frac{I_{PR}^+(t_E{}^\circ)}{p_{out}}\left(\frac{L_1}{S_1 D_1} + \frac{L_2}{S_2 D_2}\right) \tag{8}$$

ϕ_1 in eq. (7) and ϕ_2 in eq. (8) are the initial Thiele moduli for reactive layer 1 in the RP film and reactive layer 2 in PR film, respectively, and k_1 and k_2 are the corresponding initial apparent reaction rates in reactive layers 1 (RP film) and 2 (PR film), respectively. These apparent initial reaction rates correspond to $k_0 = \mu K R_0$ for the reactive monolayer.

OPTIMIZED DESIGN OF MULTILAYER FILMS

The steady-state lag time for the reactive films with consumable scavenger in eqs. (6)–(8), along with transmission rates from eqs. (57) or (60) of part II, through a purely passive barrier determine the total oxygen ingress at $t \to \infty$. When time frames of interest are finite and comparable to t_E°, the optimal barrier design corresponds to a structure with the longest t_L^+. Figure 4 shows, however, that the film with the longest t_L^+ is not necessarily the best barrier solution when the desired duration of the barrier performance is shorter than t_E°. In that case, a better transient barrier performance translates into smaller cumulative ingress values during that time. Comparing cases 2 and 3, we observe that they provide the same passive barrier at $t \to \infty$, as evidenced by the same line slope. Placing the scavenger into the inner layer material with smaller diffusivity (case 3) results in a shorter t_L^+, but the ingress during that time is much smaller than in case 2 because of the passive layer with low diffusivity protecting the reactive layer from environmental oxygen impact. Moreover, case 5, with poor barrier properties of the passive layer and a higher steady-state transmission rate through the PP film (cf. J^{PP} in Table IV), may still be preferable to case 2, with better overall passive barrier properties, if the expected barrier time (t_B) does not exceed its t_E° (ca. 36 days for case 5). This advantage is due to the placement of the scavenger into the first layer with lower solute diffusivity, which results in a much lower transient flux. Obviously, on the longer timescale after scavenger capacity exhaustion in the reactive layer, structure 2 provides a better barrier than structure 5. Thus, we found that the matrix material selection for the layer containing the scavenger largely depends on the relationship between the diffusivities of the reactive and passive layers, the desired time to provide a barrier, and its relation to the steady-state scavenger exhaustion time of the multilayer structure.

Two critical factors determining the optimal design of the RP multilayer film from a practical standpoint are thus identified: the maximum allowed cumulative oxygen ingress into the package and the desired time to reach that maximum. The optimal design of the multilayer structure incorporating a single reactive layer is found to be an RP_n film where all n passive layers can be counted as a single layer with the steady-state transmission rate ($TR^P_{1\ldots n}$) found from eq. (3). Depending on the specific values of two control factors, the choice of the matrix material for reactive layer 1 results from the solution of the modified equation [eq. (7)] for the steady-state SG model lag time

$$t_L^+ = \frac{\mu R_0}{k_1 C_1^*}\left[\frac{\phi_1^2}{2} + \ln(\cosh(\phi_1))\right] - \frac{2\mu R_0 L_1}{(1+\phi_1)p_{out}}\left(\arctan\left(e^{\phi_1} - \frac{\pi}{4} - \frac{e^{\phi_1}}{\phi_1(1+e^{2\phi_1})} + \frac{1}{2\phi_1}\right) \times \left(\frac{1}{TR_1^R} + \frac{1}{TR^P_{1\ldots n}}\right)\right. \quad (9)$$

approximately valid for $\phi_1 > 2$ and analysis of the total ingress during the desired t_B and its relationship to t_L^+. Here TR_1^R is the steady-state transmission rate through the passive matrix of the (inactive) reactive layer 1. C_1^* at the reactive side of the RP interface in eq. (9) can be determined approximately from eq. (38) of part II for the RP film with Henry's law. In general, for the case of the heterogeneous passive multilayer structure (P_n) protecting reactive layer 1, the initial C_1^i, which is the equivalent of C_1^{RP} in eq. (38) of part II, may be found from the initial partial pressure p_1^i at the RP interface by the solution of the following system of linear equations for the unknowns β_1, β_2, and p_1^i, following the steady–unsteady solution matching method described in ref. 3.:

$$\beta_1 + \beta_2 = S_1 p_{in} \quad (10)$$

$$\beta_1 e^{\phi_1} + \beta_2{}^{-\phi_1} = S_1 p_1^i \quad (11)$$

$$\sqrt{k_1 D_1}(\beta_1 e^{\phi_1} - \beta_2 e^{-\phi_1}) = TR^P_{1\ldots n}(p_{out} - p_1^i) \quad (12)$$

where β_1 and β_2 are the coefficients in the steady-state solution of the reaction–diffusion equations for permeant concentration in the catalytic reactive layer (determined from the boundary conditions). The solution of the system [eqs. (10)–(12)] has the form:

$$p_1^i = \frac{C_1^i}{S_1} = \frac{2S_1 p_{in} e^{\phi_1} + \lambda p_{out}(e^{2\phi_1} - 1)}{S_1(e^{2\phi_1} + 1) + \lambda(e^{2\phi_1} - 1)} \quad (13)$$

where the parameter λ has the dimensions of S:

$$\lambda = \frac{TR^P_{1\ldots n}}{\sqrt{k_1 D_1}} \quad (14)$$

The final C_1^f, which is the equivalent of C_1^{PP} in eq. (38) of part II, is found from p_1^f with the equality of fluxes across any plane (x = constant) in the purely passive $n + 1$ layer film

$$J_x = TR_1^R(p_1^f - p_{in}) = TR^P_{1\ldots n}(p_{out} - p_1^f) \quad (15)$$

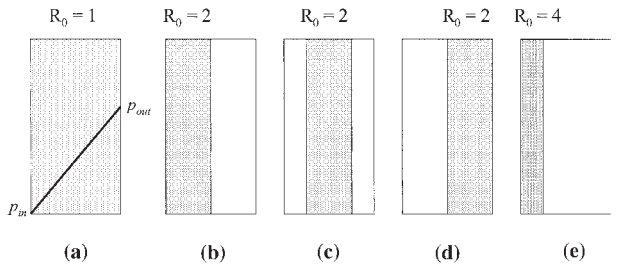

Figure 6 Potential options for scavenger placement in the homogeneous film matrix.

as

$$p_1^f = \frac{C_1^f}{S_1} = \frac{TR_{1\cdots n}^P p_{out} + TR_1^R p_{in}}{TR_{1\cdots n}^P + TR_1^R} \tag{16}$$

With eqs. (13) and (16), the arithmetic mean solute concentration C_1^* at the reactive side of the RP interface is found analogously to eq. (38) of part II as

$$C_1^* = \frac{S_1(p_1^i + p_1^f)}{2} \tag{17}$$

Equations (2), (3), (9), (13), (14), (16), and (17) provide a complete toolset for the evaluation of the ESG model t_L^+ of any RP_n film. For the ingress through the RP_n film during t_E° that includes t_L^+, eqs. (28) and (29) of part I for the monolayer reactive film should be used without modification because they do not explicitly include time and interfacial concentrations; hence, the substitution of p_1 is not necessary. Thus, a complete set of equations is developed for analysis of the SG model lag time and the ingress through practically important RP_n film structures shown to be the optimum multilayer designs for achieving the minimum ingress and maximum useful life of the scavenger.

SCAVENGER PLACEMENT IN A HOMOGENEOUS MATRIX

One of the options currently explored for the improvement of barrier performance of packaging structures involves a single-matrix material for multilayer designs with the only difference between the layers being the scavenger placement. More precisely, the same amount of scavenger can be dispersed through the entire film thickness or it can be contained within one of thinner sublayers created during melt processing, as shown in Figure 6. In all cases, the membrane is placed the same way relative to the separated environments with the left side exposed to $p_{\text{in}} = 0$ and the right side exposed to $p_{\text{out}} > 0$, as shown in the case in Figure 6(a). The cases in Figure 6(b–d) show different potential placement options of the reactive sublayer relative to separated environments versus homogeneous scavenger dispersion in the case in Figure 6(a). The case in Figure 6(e), on the other hand, demonstrates the potential for the placement of higher scavenger concentrations into thinner sublayers compared to the cases in Figure 6(a,b), whereas the total scavenger molar (weight) loading R_0AL_R is the same in all cases (where L_R is the initial thickness of the reactive layer).

The ESG model described in part II is able to solve the cases depicted in Figure 6(a,b,d,e). The case shown in Figure 6(c) can also be resolved if we combine methodologies developed for the PR and RP films into PRP film analysis. In fact, the cases in Figure 6(a,b,d) have been quantitatively analyzed earlier, and they correspond to case 7 from Table I, case 1 from Table II, and case 1 from Table III, respectively. Comparing the ESG model t_L^+ values for these cases, we observe that whereas the design in Figure 6(a) provides a better transient barrier than that in Figure 6(d), the design in Figure 6(b) is clearly superior to both of them. The design in Figure 6(c) provides intermediate barrier improvement compared to the designs in Figure 6(b,d). Rigorous derivation of this result in terms of steady-state lag times is described in ref. 11 for the case of the fast reaction $\phi_0 \gg 1$ and with modified method of Frisch for the calculation of lag times. Although interested readers may analyze the PRP film case themselves with the presented methodology, our numerical simulations have also supported this conclusion. Thus, in terms of scavenger placement into the homogeneous matrix material, we have proven that the RP design provides the best reactive barrier improvement versus the corresponding PP film. The numerical and ESG model analyses of the case shown in Figure 6(e) show that it provides better transient barrier improvement than cases shown in Figure 6(b), and the case in Figure 6(b) is better than that in Figure 6(a). Thus, the reduction of the reactive layer thickness in the RP film with the corresponding increase in the scavenger concentration in it to keep the total scavenger load constant results in improved transient barrier performance. This improvement is in line with asymptotic lag time increase, as immediately follows from eq. (36) in part I. This conclusion is based on the assumption that the increased scavenger concentration does not affect its capacity or reactivity. In real-world systems, scavenger particle agglomeration and limited oxygen access to the reactive sites are likely to limit the benefits of the RP film design as the reactive layer thickness is reduced ($L_1 \to 0$). In practice, high scavenger concentrations are unlikely to be homogeneously dispersed in thin polymer layers. Moreover, the overall transport properties of the polymer matrix may be significantly affected by the presence of large amounts of dispersed species or a high

degree of matrix polymer backbone functionalization.

PROCEDURE FOR SELECTING MATERIAL PROPERTIES OF THE REACTIVE LAYER

The layer sequence in multilayer packaging film is determined by many factors unrelated to the minimization of oxygen ingress, such as film mechanical properties, tear and puncture resistance, moisture sensitivity of the materials involved, regulatory limitations on food contact layer, gloss, and the printability of the skin layer. Most of these requirements apply to film skin layers exposed to the environment and the package contents. To simplify the task, we exclude noninterchangeable skin layers from consideration and formulate the selection procedure only for those layers that allow arbitrary sequencing within a layered laminate/coextrudate structure. The reactive layer is assumed to be one of these layers. The design goal is to achieve the minimal cumulative oxygen ingress into the package during predetermined t_B, which can also be chosen to be infinite.

As discussed earlier, the RP_n film design provides the best transient barrier performance for the case of $p_{in} = 0$. The outlined procedure allows us to determine which material to use as a matrix for the first layer loaded with the scavenger particulate. Of course, the matrix material question does not arise for functionalized polymers acting as scavengers; such polymers should always be used as the first layer (exposed to the package contents to be protected from oxygen ingress) within the material selection constraints for the food contact layer. It was shown that when layer transport properties do not depend on the presence of copermeants in the case of multicomponent diffusion, the film barrier performance (transient and steady state) is not affected by the sequence of passive layers. Hence, there are only $n + 1$ distinct design possibilities, where any of $n + 1$ layers can be used as the first layer (a matrix for the scavenger placement) and the sequencing of the other n layers is arbitrarily chosen. Each of these $n + 1$ designs should be analyzed as follows:

1. Determine the individual transmission rates (TR_i's) of the n proposed passive layers experimentally or from literature data according to eq. (2) at the intended conditions of use (temperature and relative humidity).
2. Calculate $TR^P_{1\ldots n}$ for n passive layers from eq. (3) with their individual transmission rates.
3. Calculate the average solute concentration C_1^* at the reactive side of the RP interface from eq. (17) assuming $p_{in} = 0$ (the case $p_{in} > 0$ is much more complex, as it may involve the scavenging of headspace oxygen).
4. Replace C_{out} with C_1^* in eq. (17) of part I and find t_E° with it.
5. Compare t_E° with the desired t_B:

If $t_B < t_E^\circ$, substitute t_B into eq. (16) of part I, replace C_{out} with C_1^*, and solve eq. (16) of part I for L_d. From a numerical standpoint, it may be more convenient to calculate a set of corresponding times for an array of several equally spaced L_d values [0 … L_1] and then interpolate the resulting times to obtain $L_d(t_B)$. Then, let the dimensionless wavefront position $\xi^* = L_d(t_B)/L_1$ and use the analytical result [eq. (28) of part I] or numerically solve eq. (25) of part I to calculate the total ingress $I_R^+(t_B)$.

If $t_B \geq t_E^\circ$, use eq. (29) of part I to find $I_R^+(t_E^\circ)$ and use the modified equation [eq. (24) of part I] to find the ingress after t_E°:

$$I_P(t_B - t_E^\circ) = TR^P_{total} p_{out}(t_B - t_E^\circ) \tag{18}$$

where TR^P_{total} is the steady-state transmission rate through all $n + 1$ layers, including inactive reactive layer 1 (the transmission rate through its passive matrix):

$$TR^P_{total} = \frac{1}{\dfrac{1}{TR^P_{1\ldots n}} + \dfrac{1}{TR^R_1}} = \frac{1}{\dfrac{1}{TR^P_{1\ldots n}} + \dfrac{L_1}{D_1 S_1}} \tag{19}$$

Then, the total ingress $I^+(t_B)$ is found as

$$I^+(t_B) = I_R^+(t_E^\circ) + I_P(t_B - t_E^\circ) \tag{20}$$

ϕ_0 for the reactive film in eqs. (28) and (29) of part I is the equivalent of ϕ_1 for the RP film and now refers to the initial Thiele modulus of the fully activated reactive layer 1 in the RP_n structure:

$$\phi_0 = L_1 \sqrt{\frac{\mu K_1 R_{01}}{D_1}} \tag{21}$$

This procedure should be repeated for all $n + 1$ distinct barrier designs: the optimal design will correspond to the lowest $I^+(t_B)$. If one considers that oxygen solubility varies only slightly in most rubbery and many semicrystalline polymers compared to its diffusivity, the number of repeat steps can be reduced with the following rule of thumb. The best overall transient barrier performance (defined without referring to a specific t_B as the solute ingress during the scavenger exhaustion time) is obtained when the scavenger is placed into layer 1 and the matrix material of layer 1 has the lowest oxygen diffusivity of all materials considered for multilayer structure. This design, called the *primary design*,

however, will have the shortest scavenger exhaustion time among the RP_n films. By choosing the primary design and evaluating its t_E° according to the outlined procedure, one can get an idea how the resulting t_E° compares with the required t_B. Because all other RP_n film designs cannot significantly extend the obtained t_E° but they will result in reduced barrier performance during that t_E° (taken as a fixed parameter of the primary design), the evaluation of the primary design t_E° immediately establishes whether the choice of layer materials and their thicknesses is appropriate for obtaining the desired barrier performance. If the expected t_B is significantly longer than t_E° for the primary design, the transient barrier improvement due to the scavenging reaction is unlikely to meet the design expectations. After all, the total amount of oxygen consumed by the noncatalytic scavenger is always equal to $\mu R_0 A L_R$ or $\mu_m m_s$ (where μ_m is the bulk scavenger reactive capacity per unit mass of scavenger and m_s is the mass of the scavenger loaded into the layer matrix). This oxygen amount can be prevented from entering the package or consumed from the package contents (product and headspace) or can undergo some combination of both. The RP_n film design is shown to be the best for minimizing the oxygen ingress. The significant presence of headspace oxygen, resulting in a bidirectional flow of oxygen into the scavenging layer and the change of design goal from ingress reduction to scavenging the most headspace oxygen, may drastically change the optimal design. The point is easily demonstrated if one of the layers is an absolute barrier to oxygen permeation. Then, it obviously makes no sense to place the scavenger into this layer: such a layer should be made the outer layer exposed to the environment, whereas the scavenging layer could be one of the internal layers. The scavenger will then only consume the headspace oxygen, which will result in the full utilization of the scavenger reactive capacity and the highest efficiency of oxygen removal (if the scavenging layer is exposed to the package contents). Such a situation is beyond the scope of this work, which is focused on improving the transient barrier to oxygen permeation through chemical reaction and multilayer film design when none of the layers acts as an absolute barrier to permeation.

To present a detailed account of transient permeation, the presented discussion has been intentionally limited to a single permeant, and the material transport properties have been assumed to be independent of solute concentrations. In reality, the presence of copermeants, such as other atmospheric gases and water vapor, can significantly affect the kinetic and thermodynamic transport properties of the polymeric materials. For example, if the materials used in some layers are moisture sensitive, the presented procedure has to be modified to account for material transport property dependence on relative humidity within each layer. A simple approach may use the average humidity within each layer obtained by the application of the standard steady-state transmission rate method for water vapor transport through a multilayer structure and determining the water vapor concentrations at all layer interfaces. Then, the average humidity of the layer can be taken as an arithmetic mean of the interfacial concentrations at the layer boundaries. The average humidity of each layer in a particular layer sequence can be used to determine the TR_i's of the solute of interest across each layer. These transmission rates are subsequently substituted into Step 1 of the outlined procedure for the analysis of each RP_n film design.

CONCLUSIONS

In part III, we have presented specific cases of ingress dynamics analysis through RP and PR films. Then, we extended the SG model of transient permeation and ingress to include arbitrary multilayer film designs when one of the layers contained a noncatalytic immobile solute scavenger. The novel methodology for the analysis of the ingress dynamics and the optimized designs of multilayer reactive barrier solutions were presented to include layer sequencing, layer property selection, and practical recommendations for scavenger placement in the polymer matrix. The methodology can be applied to the practical design of multilayer packaging films containing oxygen scavengers within one of the layers and the comparative barrier performance analysis of existing active packaging structures.

NOMENCLATURE

Additional relevant nomenclature is included in parts I and II of this series of articles.

L_R initial thickness of the reactive layer (m)
m_s mass of scavenger loaded into the film layer (kg)
V volume of downstream chamber or package (m^3)

Greek symbols

γ initial barrier improvement ratio in terms of effective flux [$= J^P/J_0(0)$]
ε barrier improvement ratio in terms of cumulative ingress [$= I_R(t_E^\circ)/I_P(t_E^\circ)$] during t_E° due to scavenging reaction
λ coupling parameter in eq. (13) as defined in eq. (14) for the determination of the partial interfacial pressure of the solute in a RP_n film [cm^3 (STP) m^{-3} Pa^{-1}]

μ_m bulk reactive capacity of the scavenger (moles of solute scavenged per scavenger unit weight; mol/kg)

References

1. Solovyov, S. E.; Goldman, A. Y. J Appl Polym Sci 2006, 100, 1940.
2. Solovyov, S. E.; Goldman, A. Y. J Appl Polym Sci 2006, 100, 1952.
3. Solovyov, S. E.; Goldman, A. Y. Int J Polym Mater 2005, 54, 71.
4. Solovyov, S. E.; Goldman, A. Y. Int J Polym Mater 2005, 54, 93.
5. Solovyov, S. E.; Goldman, A. Y. Int J Polym Mater 2005, 54, 117.
6. Siegel, R. A. J Phys Chem 1991, 95, 2556.
7. Barrie, J. A.; Levine, J. D.; Michaels, A. S.; Wong, P. Trans Faraday Soc 1963, 59, 869.
8. Yang, C.; Nuxoll, E. E.; Cussler, E. L. AIChE J 2001, 47, 295.
9. Crank, J. The Mathematics of Diffusion, 2nd ed.; Clarendon: Oxford, 1975.
10. Solovyov, S. E.; Goldman, A. Y. e-Polymers 2004, 23, 1.
11. Siegel, R. A.; Cussler, E. L. J Membr Sci 2004, 229, 33.